Generation of bright squeezed light at 1.06 μm using cascaded nonlinearities in a triply resonant cw periodically-poled lithium niobate optical parametric oscillator

K. S. Zhang, T. Coudreau,* M. Martinelli, A. Maître, and C. Fabre
Laboratoire Kastler Brossel, Université Pierre et Marie Curie, case 74, 75252 Paris cedex 05, France
(Received 27 February 2001; published 20 August 2001)

We have used an ultralow threshold continuous-wave optical parametric oscillator (OPO) to reduce the quantum fluctuations of the reflected pump beam below the shot noise limit. The OPO consisted of a triply resonant cavity containing a periodically poled lithium niobate crystal pumped by a Nd:YAG (yttrium aluminum garnets) laser and giving signal and idler wavelengths close to 2.12 μm and a threshold as low as 300 μW. We detected the quantum fluctuations of the pump beam reflected by the OPO using a slightly modified homodyne detection technique. The measured noise reduction was 30% (inferred noise reduction at the output of the OPO 38%).

DOI: 10.1103/PhysRevA.64.033815 PACS number(s): 42.65.Yj, 42.50.Dv

I. INTRODUCTION

Continuous-wave optical parametric oscillators (OPOs) have been used for over a decade to study and modify the quantum noise of light. Successful experiments involved creation of squeezed light below the oscillation threshold [1,2], subshot noise intensity correlations between signal and idler beams [3,4], and pump squeezing [5]. These experiments have been performed using OPOs pumped with visible light, generally the second harmonic of Nd:YAG (yttrium aluminum garnets) lasers, and most of them generated nonclassical light at a wavelength different from the pump wavelength. Pump squeezing in an OPO above threshold [5] provides a direct and efficient way to generate bright squeezed beams without frequency changes. The OPO acts as a ''quantum noise eater,'' like a Kerr medium, by making use of the so-called ''cascaded nonlinearities'' [6]. Such cascaded nonlinearities, resulting from the coexistence of sum-frequency generation and parametric down conversion occurring in an OPO, have been shown to amount to a nonlinear phase shift on the pump beam which emerges from the cavity after its nonlinear interaction with the signal and idler beams in the parametric crystal. This effect has been known for a long time to be able to produce significant quantum noise reduction [7]. In order to have access to a new frequency range in pump squezing, we have used a quasi phase-matched (QPM) material, periodically poled lithium niobate (PPLN), which makes it possible to build low-threshold cw OPOs operating with a Nd:YAG laser as a pump and signal and idler beams in the mid-IR [8–10]. The experiment that we present here is the first, to the best of our knowledge, to use QPM material for a quantum noise reduction experiment in the cw regime.

After a brief description of the experimental setup, we will study in Sec. III the behavior of the mean fields produced by this device and compare it to theoretical predictions. In Sec. IV we will present the theoretical predictions as well as the experimental results for the quantum noise, showing 38% noise reduction below the standard quantum limit.

II. EXPERIMENT SETUP

The setup is shown on Fig. 1. We have used a diode-pumped monolithic Nd:YAG laser (Lightwave 126-1064-700) as a pump source. This source delivers a cw beam in a TEM_{00} mode which exhibits very large excess noise below 20 MHz due to the relaxation oscillation peak noise of the pump semiconductor laser (left, Fig. 2). In order to obtain noise reduction below the standard quantum limit within the OPO cavity bandwidth, we need first to obtain a pump beam at the shot-noise level. For this purpose we send the beam through a filtering cavity. It is a ring three-mirror cavity [11] to prevent back reflections from perturbing the laser (Fig. 1). The input and output mirrors ($M1$,$M2$) are identical plane mirrors with a reflexion coefficient on the order of 99.5% for the *s*-polarization. The end mirror ($M3$) is a concave mirror with a radius of curvature of 750 mm and a reflexion coefficient close to 99.9%. The measured finesse for the cavity is close to 700. For a 70-cm round-trip length the cavity bandwidth is below 1 MHz when the cavity is locked on resonance. The field fluctuations of the transmitted beam are shot-noise limited above 5 MHz (right, Fig. 2). Due to the non-negligible losses on the mirrors, we obtain 30% power transmission as opposed to 80% theoretical prediction and 75% in similar experiments where very-high-quality mirrors were used [11]. When the cavity is locked by a servo loop using a frequency modulation of the Nd:YAG laser at 40 kHz, its output is stable over several tens of minutes. The mode matching of the pump beam to the OPO cavity was 92% without the filtering cavity and over 97% with the filtering cavity which plays a role of spatial filter.

The half wave plate HWP1 and the polarizing beam splitter PBS1 control the pump intensity sent into the OPO cavity. The pump beam passes through the Faraday rotator (FR), and the input polarization is controlled by the half wave plate HWP2. The reflected pump beam, after the interaction with the OPO cavity, returns by the same optics and is reflected by PBS1 after the double passage through the Faraday rotator. For the local oscillator, we used part of the input beam re-

*Author to whom correspondence should be addressed. Email address: coudreau@spectro.jussieu.fr

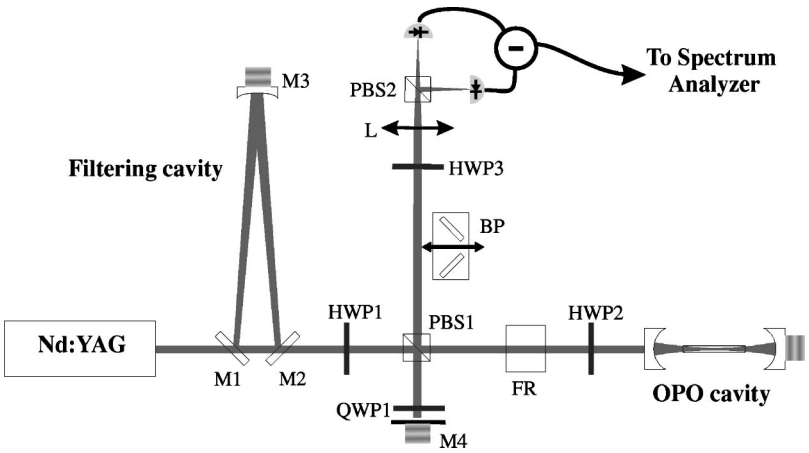

FIG. 1. Experimental setup.

flected by PBS1. The reflected beam passes by an optical circulator made by a quater wave plate (QWP1) and a mirror ($M4$) mounted in a piezoactuator for the phase variation. The crossed polarized local oscillator and reflected pump beams are then mixed at the homodyne detection system by the polarizing beam splitter PBS2 and the half wave plate HWP3, and detected by the high efficiency InGaAs photodetectors (Epitaxx ETX 300, quantum efficiency 94%). A pair of Brewster plates (BP) at the Brewster angle for the local oscillator polarization can be introduced in the system, producing a reduction in the reflected pump beam with no noticeable change in the local oscillator.

The triply resonant OPO has been described extensively in a previous paper [8] and we will only recall here its main properties. The cavity is a symmetric cavity with a length of approximately 65 mm. The pump coupling mirror ($M5$) has a reflection coefficient of 87%, so that the transmission is much larger than the other losses inside the cavity. The end mirror ($M6$) is highly reflecting for the pump beam to reduce the losses (reflection of 99.8%). The mirrors have large reflection coefficients in the 2-μm range to ensure small losses for the pump beam due to conversion to signal and idler (99.8% for $M5$, 99% for $M6$). They have a radius of curvature of 30 mm to ensure optimal waist sizes in the crystal (36 μm at 1.06 μm, 51 μm at 2.12 μm).

The crystal is a PPLN crystal from Crystal Technologies, with a width of 12 mm, a length of 19 mm, and a thickness of 0.5 mm. Both faces of the crystal are antireflection coated for pump, signal, and idler frequencies (residual reflection of 0.6% for the pump and 0.4% for signal and idler). The crystal absorption in the infrared region is small (0.3% at 1.06 μm according to the manufacturer). The crystal is formed of eight different paths with spatial periodicity varying between 30 and 31.2 μm. All the experimental results shown in this paper were made using a 31.1 μm spatial period for which the exact quasi-phase-matching condition for degenerate signal and idler wavelength at 2.12 μm is obtained with a temperature $T_{\mathrm{QPM}} \approx 162\,^{\circ}\mathrm{C}$. The crystal is placed inside a temperature stabilized oven. In the presence of the crystal, the measured finesse for the pump is around 40, in good agreement with the theoretical expressions while the calculated finesse for signal and idler is around 200. The typical oscillation threshold is around 500 μW with thresholds as low as 300 μW for a limited time. For continuous operation, the OPO cavity is locked in the resonance of the 2 μm output.

III. MEAN-FIELDS STUDY

The well-known equations for the intracavity mean fields are [12]

$$E_0 = t_0 E_{in} + r_0 (E_0 - \chi^* E_1 E_2) e^{i\varphi_0}, \tag{3.1}$$

$$E_1 = r (E_1 + \chi E_0 E_2^*) e^{i\varphi_1}, \tag{3.2}$$

$$E_2 = r (E_2 + \chi E_0 E_1^*) e^{i\varphi_2}, \tag{3.3}$$

where E_0, E_1, and E_2 are the intracavity pump, signal, and idler fields, respectively, t_0 and r_0 are the amplitude trans-

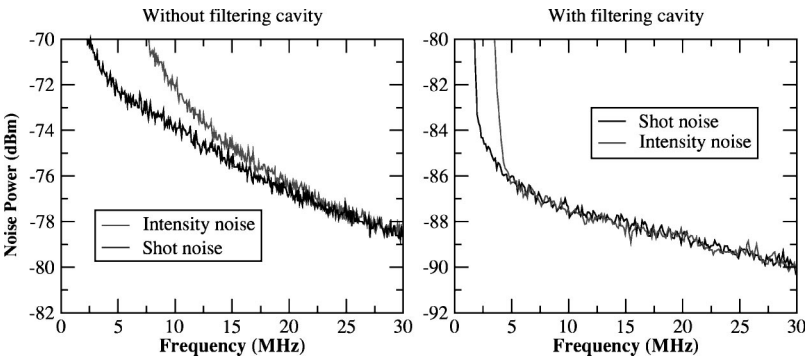

FIG. 2. Intensity noise before and after the filtering cavity showing that the output beam is shot-noise limited above 5 MHz.

mission and reflection coefficients at the pump frequency, χ is the nonlinear coupling coefficient, and r is the common value for the amplitude reflection coefficient at the signal and idler frequencies. φ_0, φ_1, and φ_2 are the round-trip phases for pump, signal, and idler fields, respectively. Above threshold, Eqs. (3.2) and (3.3) lead to the condition [13]

$$\varphi_1 = \varphi_2 + 2p\pi, \tag{3.4}$$

where p is an integer. Each value of p is associated with a given mode, i.e., a well-defined couple of signal and idler frequencies, ω_1 and ω_2. More precisely, using the Sellmeier equation for lithium niobate [14] and Eq. (3.4), one can find for any given cavity length L_{cav}, crystal temperature T, and mode index p the values of ω_1 and ω_2. T and p being fixed, a minimum of the oscillation threshold is reached at values of the cavity length where both φ_1 and φ_2 are multiples of 2π. Let us call L_p the signal-idler double resonance point within a given free spectral range.

In order to calculate the oscillation threshold and output fields, we have taken into account the periodical poling. The usual phase mismatch, $\Delta k = k_0 - k_1 - k_2$, is replaced by $\Delta\kappa = k_0 - k_1 - k_2 - 2\pi/\Lambda$, where Λ denotes the spatial period of the crystal. The nonlinear coupling coefficient, which can be written in a usual bulk crystal

$$\chi = \chi^{(2)}_{bulk} = \chi^{(2)}\left(\omega_0, \frac{\omega_0}{2}, \frac{\omega_0}{2}\right) \mathrm{sinc}\left(\frac{\Delta k l}{2}\right) \exp\left(-i\frac{\Delta k l}{2}\right), \tag{3.5}$$

with $\mathrm{sinc}(\varphi) = \sin(\varphi)/\varphi$, now becomes

$$\chi = \chi^{(2)}_{QPM} = \chi^{(2)}\left(\omega_0, \frac{\omega_0}{2}, \frac{\omega_0}{2}\right) \frac{2}{\pi} \mathrm{sinc}\left(\frac{\Delta\kappa l}{2}\right) \exp\left(-i\frac{\Delta\kappa l}{2}\right) \tag{3.6}$$

for an integer number of periods within the crystal of length l. If the crystal does not consist of an integer number of periods, the coupling coefficient has an additional term like $\chi^{(2)}_{bulk}$, depending on the added fraction of the period. Since the relative contribution of this term will have the order of Λ/L, it can be neglected in the calculation of $\chi^{(2)}_{QPM}$. However, its contribution to the crystal length will have a much more important effect in the relative phase shift between the interacting beams. The effect of such an additional phase shift is known to increase the threshold in the case of a linear OPO cavity [13]. This increase will depend on this phase term, reaching 1.9 times the mininum threshold that would be obtained with a perfect phase matching, perfect periodicity of the crystal, and no added relative phase. In order to optimize the threshold, it is possible to use crystals with nonparallel faces that allow a precise choice of the crystal length [15,16].

The curves in Figs. 3(d)–3(f) show the mean-field intensities calculated from these equations as a function of cavity length for three different temperatures and pump intensities. For a given cavity length, there are many different modes p where the OPO can oscillate. For each one of these modes there will be a different threshold value, and the OPO will operate in the mode with the lowest threshold [17]. The calculated frequency difference between signal and idler is shown in THz on traces 3(a), 3(b), and 3(c) showing that the system can be swept over a large frequency range. During the cavity scanning, the OPO passes through a large number of individual modes, remaining on a given value of the frequency difference only over a limited range of cavity length [inset, curve 3(a)]. When the temperature approaches T_{QPM}, the signal and idler frequencies become very close, and the difference between signal and idler indices of refraction becomes very small. In these conditions, the resonance lengths L_p of different oscillation modes p become very close to each other and the possible oscillating modes overlap. As the OPO is never multimode in steady-state operation [17,18], it jumps from one mode to the next ($p \rightarrow p \pm 2$) when the cavity length is varied. As a result, the OPO always oscillate very close to the double resonance configuration. The mode jumps can be seen as discontinuities on the mean field. These discontinuies are easily visible on the experimental curves and using an auxiliary Fabry-Perot, we have observed monomode operation with mode hops at the discontinuities. These discontinuities are not seen on the calculated curves which do not take into account the dynamics of the system while experimentally, since the threshold varies slowly for the different modes, the OPO remains on its initial mode even if it is unstable, leading to mode jumps by more than two units.

Intracavity signal and idler intensities exhibit a bistable behavior as a function of cavity length when specific conditions on the pump and signal detunings are met [19]. In our case, as the OPO works almost always with a small detuning of the signal and idler fields, it is difficult to observe any bistable behavior. Nevertheless, due to the parabolic shape of the phase-matching curve in a type-I medium [20], for a temperature close to T_{QPM}, oscillation is limited by the frequency degeneracy of signal and idler ($p = 0$). Thus the detuning range obtained for the mode $p = 0$ is much larger than that obtained for other modes. Such a behavior may be seen on the left-hand side of curve 3(f). In this region, for an adequate cavity detuning the bistable behavior is expected. The value of the pump detuning can be selected by the temperature control of the phase matching condition at degeneracy, displacing the position of the sharp side of the signal and idler curve relative to the pump resonance position. The sharp edge position is critically dependent on the temperature, and a 0.1 °C variation is enough to displace the degenerate point out of the pump resonance.

IV. QUANTUM FLUCTUATIONS OF THE PUMP FIELD

The quantum fluctuations of the pump field have been calculated in Ref. [21]. This paper shows that best quadrature squeezing on the pump field increases with pump power and is already significant a few times (by a factor 3 or 4) above threshold and for any value of the detunings. It increases when approaching the bistability threshold, i.e., for rather important signal-idler and pump detunings. Squeezing occurs on the phase component at exact double resonance [5] and, for nonzero detunings, on a quadrature component that rotates quickly when this detunning changes. Using the detailed calculations of [21], it is possible to evaluate the opti-

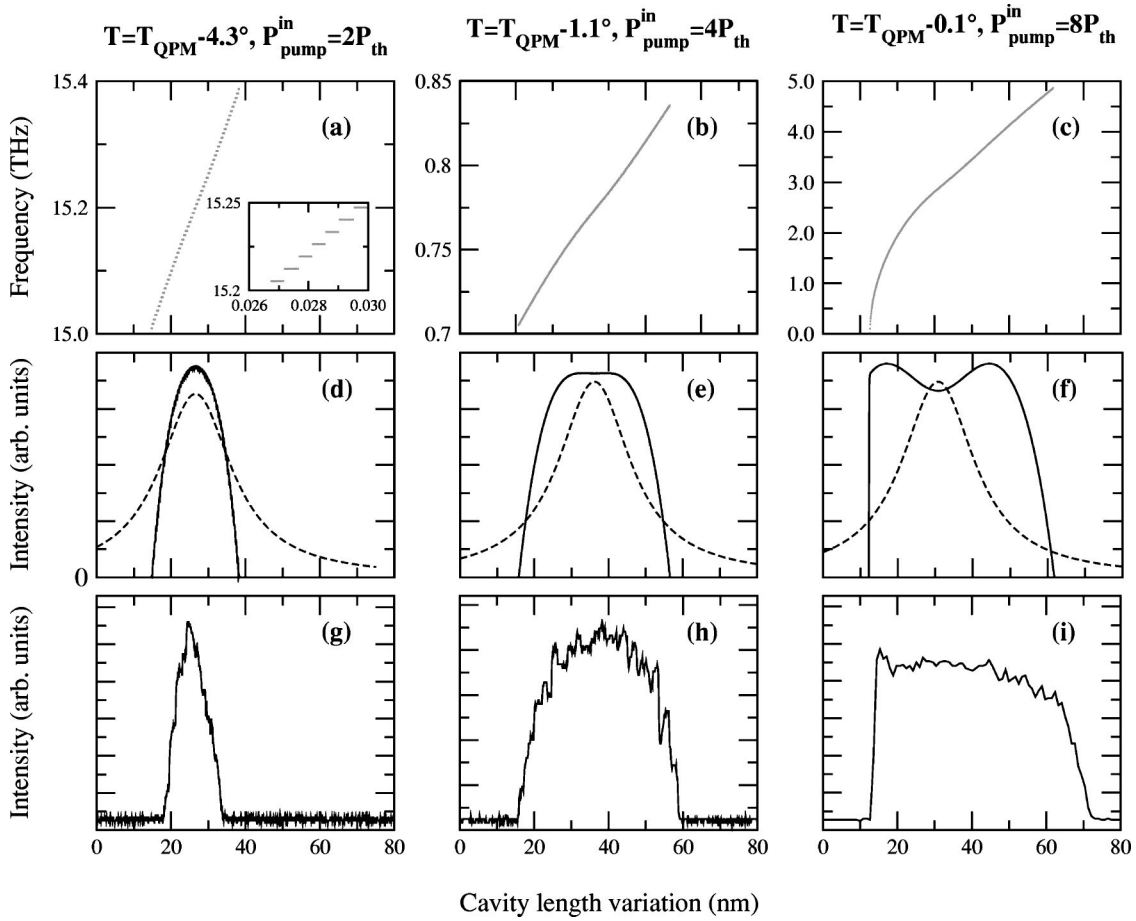

FIG. 3. OPO mean values study as a function of the variation of cavity length. The frequency difference between the signal and idler in THz is shown on traces (a), (b), and (c). Calculated signal mean intensities [traces (d), (e), (f), continuous line] and experimental curves [traces (g), (h), (i)] are shown with the same scales; the undepleted pump mean intensity is shown for comparison (dashed lines). The horizontal axis is in μm. The experimental conditions (temperature and pump power) are $T=T_{\mathrm{QPM}}-4.3°$ and $P^{in}_{pump}=2P_{th}$ [traces (a), (d), and (g)], $T=T_{\mathrm{QPM}}-1.1°$ and $P^{in}_{pump}=4P_{th}$ [traces (b), (e), and (h)] and $T=T_{\mathrm{QPM}}-0.1°$ and $P^{in}_{pump}=8P_{th}$ [traces (c), (f), and (g)]. P_{th} is the minimum threshold obtained at exact resonance for pump, signal, and idler at a given temperature. In curve (a) the zoom area shows the mode hop during the cavity scan.

mum noise reduction as a function of cavity length at a given temperature. The curves are shown in Fig. 4. It can be seen on these curves that the optimum squeezing is significant on a broad range of detunings and increases with the pump power. On the other hand, the intensity noise (gray line) exhibits rapid oscillations for small changes of the cavity length (of the order of tenths of nm). Even with a stable electronical locking of the OPO cavity, fast small variations around the locking position cannot be avoided, thus reducing the measurable intensity squeezing. Actually the most efficient locking is obtained exactly at the triply resonant condition when only quadrature squeezing can be observed.

The quantum noise of quadrature components of the reflected pump beam are measured using a slightly modified homodyne detection procedure. In order to prevent saturation of the detectors (which occurs around 3 mW), the local oscillator cannot be much more powerful than the reflected pump beam. The difference of the photocurrents fluctuations obtained by the two balanced photodetectors can be written as

$$\Delta^2(i_1-i_2)\propto I_{LO}\Delta^2 E_\theta \tag{4.1}$$

only when the local oscillator is much stronger than the beam to measure. I_{LO} denotes the mean local oscillator power and $\Delta^2 E_\theta$ the variance of the reflected pump in the quadrature θ determined by the phase difference between the local oscillator and the reflected pump mean field. The measurement, with a spectrum analyzer, of the spectral density of the difference of the photocurrents gives directly the noise spectrum of the quadrature component of angle θ. In the general case of a finite ratio between the mean intensities of the beam to study and of the local oscillator beam, an additionnal term appears and the difference of the photocurrents is now

$$\Delta^2(i_1-i_2)\propto I_{LO}\Delta^2 E_\theta + I\Delta^2 E_{LO,p}, \tag{4.2}$$

where we neglect correlations between the two beams (this is justified since these beams are obtained by splitting a coherent state on a beam splitter). I is the mean reflected pump

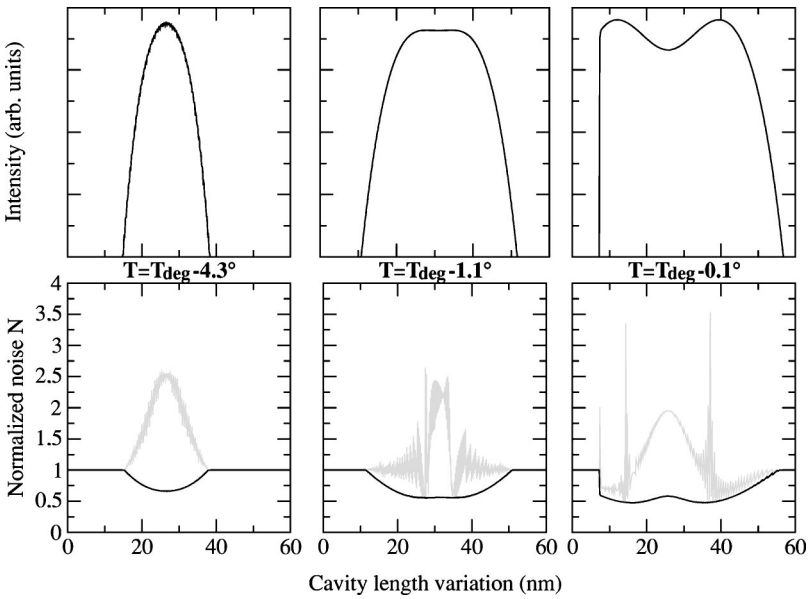

FIG. 4. Calculated mean intensities (upper traces) and noise (lower traces; dark line, optimum noise reduction; gray line, intensity noise) as a function of cavity length in the same conditions as Fig. 3.

intensity and $\Delta^2 E_{LO,p}$ the variance of the pump beam in a given quadrature. This extra term can be measured independently. Taking into account the fact that the local oscillator is in a coherent state, its high-frequency noise is equal to that of the vacuum noise and can be measured by blocking the local oscillator arm. Using this measurement, we can renormalize the total photocurrent difference (4.2) and obtain the reflected pump noise. This correction amounts to approximately 30% of the shot noise.

The noise measurement is made with a pair of balanced InGaAs photodetectors. The mode matching between the reflected pump and the local oscillator is on the order of 97%. The pump intensity incident on the OPO is $P_{pump}^{in}=1.2$ mW, for a threshold power of 300 μW. The reflected pump intensity at the position of the photodetectors was $P_{pump}^{det}=0.45$ mW. The temperature is $T=T_{\mathrm{QPM}}-1\,^{\circ}\mathrm{C}$ and the local oscillator power is $P_{LO}=1.2$ mW. Figure 5 shows the noise power N_1 obtained as the local oscillator phase is scanned (thick black line), as well as the shot noise level measured for the local oscillator and the reflected pump beams (respectively, N_2 and N_3). The sum of the shot noise power of both beams is also presented for comparison. The

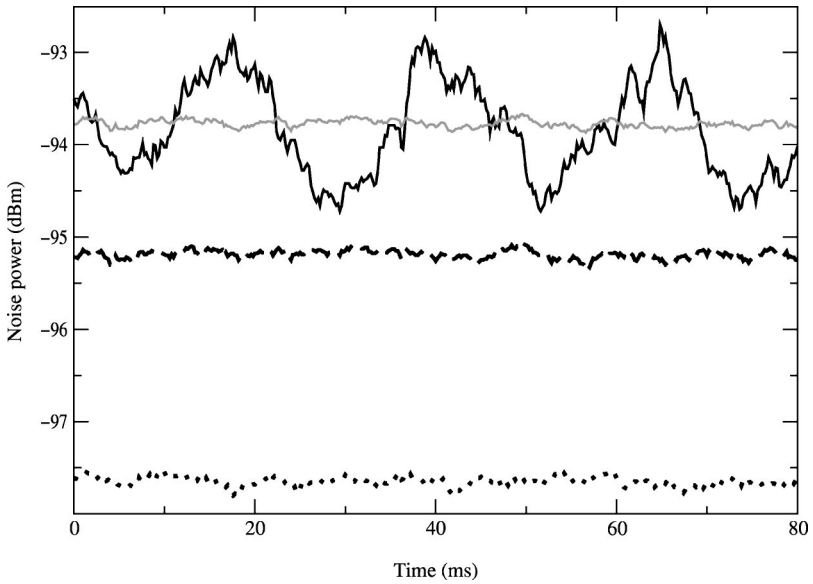

FIG. 5. Noise power measured at the homodyne detection. The thick black line is obtained with both local oscillator and reflected pump during the scan of the local oscillator phase. The dashed line is the local oscillator shot-noise level, obtained for a blocked pump. The dotted line is the shot-noise level for the reflected pump (blocked local oscillator). The gray line is the calculated shot-noise level obtained from the sum of the local oscillator and the equivalent reflected pump shot-noise power and corresponds to the expected shot noise with the two beams present (since the beams have uncorrelated fluctuations). The electronic background noise level is -102.6 dBm. The experimental conditions are the following: $P_{pump}^{in}=1.2$ mW, $P_{pump}^{det}=0.45$ mW, $P_{LO}=1.2$ mW. The experimental settings of the spectrum analyzer are as follows: the noise analysis frequency is 6 MHz, the resolution bandwidth is 100 kHz, and the video bandwidth is 10 kHz.

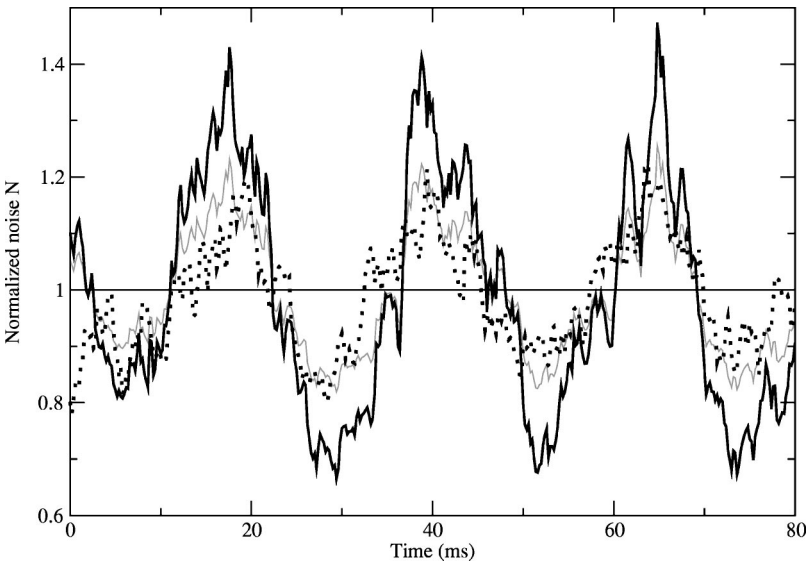

FIG. 6. Normalized noise as a function of time when the local oscillator phase is scanned. The thick black line is the unattenuated beam noise showing 30% noise reduction below the standard quantum limit. The dashed line shows the measured noise in the presence of the pair of Brewster plates. The gray line is the calculated noise taking into account the losses introduced by the pair of Brewster plates. The thin black line corresponds to the shot-noise limit.

electronic noise level is small (-102.6 dBm) and is taken into account in our calculations. The variance of the quadrature component fluctuations, normalized to the coherent state fluctuations ($N=\Delta^2 E_\theta/\Delta^2 E_{LO,p}$) can be obtained from the noise measurements shown at Fig. 5 using the correction presented in Eq. (4.2). Figure 6 shows this normalized noise $N=(N_1-N_3)/N_2$. The measured noise reduction is 30% corresponding to an inferred noise reduction at the output of the OPO of 38%, when losses are taken into account.

To check that we have indeed noise reduction below the standard level, we have introduced losses on the squeezed beam. In order for these losses not to change the operating conditions (namely the incident pump power, P_{pump}^{in}), we have introduced losses using a pair of glass plates oriented at the Brewster angle with respect to the propagation axis (Fig. 1): in that case, the losses are 46% for the squeezed beam and not measurable for the local oscillator since the two beams are orthogonally polarized. The dashed gray line of Fig. 6 gives the quadrature noise measured using this device. This line coincides well with the full gray line that represents the measured noise without attenuation (thick black line) corrected using the well-known formula [22] $N_{loss}=(1-\Gamma)N+\Gamma$, where N_{loss} is the normalized noise of the attenuated beam, N is the normalized noise of the input beam, and Γ is the loss coefficient of the inserted attenuator.

The measured noise reduction is in good agreement with the quadrature noise reduction obtained in our theoretical calculations (44%, Fig. 4). The smaller value for the measured compression may be due to an underestimated value for the intracavity losses at our calculations.

V. CONCLUSION

We have reported on the use of quasi-phase-matched materials for cw quantum noise reduction experiments and observed an inferred noise reduction of 38% below the standard quantum limit using such a material. The use of quasi-phase-matched materials in quantum optics seems very promising as it enlarges the wavelength range where quantum effects can be obtained.

ACKNOWLEDGMENTS

M.M. wishes to thank Coordenação de Aperfeiçoamento de Pessoal de Nível Superior (CAPES-BR) for funding. This research was performed in the framework of the EC ESPRIT Contract No. ACQUIRE 20029.

[1] E.S. Polzik, J. Carri, and H.J. Kimble, Phys. Rev. Lett. **68**, 3020 (1992).
[2] K. Schneider, R. Bruckmeier, H. Hansen, S. Schiller, and J. Mlynek, Opt. Lett. **21**, 1396 (1996).
[3] A. Heidmann, R.J. Horowicz, S. Reynaud, E. Giacobino, and C. Fabre, Phys. Rev. Lett. **59**, 2555 (1987).
[4] J. Mertz, T. Debuisschert, A. Heidmann, C. Fabre, and E. Giacobino, Opt. Lett. **16**, 1234 (1991).
[5] K. Kasai, JiangRui Gao, and C. Fabre, Europhys. Lett. **40**, 25 (1997).
[6] A.G. White, J. Mlynek, and S. Schiller, Europhys. Lett. **35**, 425 (1996).
[7] S. Reynaud, C. Fabre, E. Giacobino, and A. Heidmann, Phys. Rev. A **40**, 1440 (1989).
[8] M. Martinelli, K. S. Zhang, T. Coudreau, A. Maître, and C. Fabre, J. Opt. A: Pure Appl. Opt. **3**, 300 (2001).
[9] D. Serkland, R. Eckardt, and R. Byer, Opt. Lett. **19**, 1046 (1994).
[10] U. Strössner, A. Peters, J. Mlynek, S. Schiller, J.-P. Meyn, and R. Wallenstein, Opt. Lett. **24**, 1602 (1999).
[11] B. Willke, N. Uehara, E.K. Gustafson, R.L. Byer, P. King, S. Seel, and R.L. Savage, Jr., Opt. Lett. **23**, 1704 (1998).
[12] C. Fabre, in *Advanced Photonics with Second-order Optically Nonlinear Processes*, edited by A.D. Boardman *et al.* (Kluwer

Academic Publishers, Dordrecht, 1999).
[13] T. Debuisschert, A. Sizmann, E. Giacobino, and C. Fabre, J. Opt. Soc. Am. B **10**, 1668 (1993).
[14] D.H. Jundt, Opt. Lett. **22**, 1553 (1997).
[15] I. Juwiler, A. Arie, A. Skliar, and G. Rosenman, Opt. Lett. **24**, 1236 (1999).
[16] G. Imeshev, M. Proctor, and M.M. Fejer, Opt. Lett. **23**, 165 (1998).
[17] C. Schwob, P.-F. Cohadon, C. Fabre, M. Marte, H. Ritsch, A. Gatti, and L. Lugiato, Appl. Phys. B: Lasers Opt. **66**, 685 (1998).
[18] C. Fabre, M. Vaupel, N. Treps, P.-F. Cohadon, C. Schwob, and A. Maître, C. R. Acad. Sci. Ser. IV , 553 (2000).
[19] L.A. Lugiato, C. Oldano, C. Fabre, E. Giacobino, and R.J. Horowicz, Nuovo Cimento D **10**, 959 (1988).
[20] R.C. Eckardt, C.D. Nabors, W.J. Kozlovky, and R.L. Byer, J. Opt. Soc. Am. B **8**, 646 (1991).
[21] C. Fabre, E. Giacobino, A. Heidmann, L. Lugiato, S. Reynaud, M. Vadacchino, and Wang Kaige, Quantum Opt. **2**, 159 (1990).
[22] G. Grynberg, A. Aspect, and C. Fabre, *Introduction aux Lasers et à l'Optique Quantique* (Ed. Ellipses, Paris, 1997).